SCIENTIFIC REPORTS

OPEN

SUBJECT AREAS:
ANGIOGENESIS
VASCULAR BIOLOGY
STEM CELLS
METABOLOMICS

Received
21 June 2011

Accepted
8 August 2011

Published
30 August 2011

Correspondence and requests for materials should be addressed to M.F. (friedlan@scripps.edu)

* These authors equally contributed to this work.

Differential Macrophage Polarization Promotes Tissue Remodeling and Repair in a Model of Ischemic Retinopathy

Valentina Marchetti[1]*, Oscar Yanes[2]*, Edith Aguilar[1], Matthew Wang[1], David Friedlander[1], Stacey Moreno[1], Kathleen Storm[5], Min Zhan[5], Samia Naccache[3], Glen Nemerow[3], Gary Siuzdak[2,4] & Martin Friedlander[1]

[1]Department of Cell Biology, The Scripps Research Institute, La Jolla, CA, 92037, [2]Department of Molecular Biology, The Scripps Research Institute, La Jolla, CA, 92037, [3]Department of Immunology, The Scripps Research Institute, La Jolla, CA, 92037, [4]Scripps Center for Mass Spectrometry, The Scripps Research Institute, La Jolla, CA, 92037, [5]Source MDX, Boulder, CO, USA.

Diabetic retinopathy is the leading cause of visual loss in individuals under the age of 55. Umbilical cord blood (UCB)–derived myeloid progenitor cells have been shown to decrease neuronal damage associated with ischemia in the central nervous system. In this study we show that UCB-derived CD14$^+$ progenitor cells provide rescue effects in a mouse model of ischemic retinopathy by promoting physiological angiogenesis and reducing associated inflammation. We use confocal microscopy to trace the fate of injected human UCB-derived CD14$^+$ cells and PCR with species-specific probes to investigate their gene expression profile before and after injection. Metabolomic analysis measures changes induced by CD14$^+$ cells. Our results demonstrate that human cells differentiate *in vivo* into M2 macrophages and induce the polarization of resident M2 macrophages. This leads to stabilization of the ischemia-injured retinal vasculature by modulating the inflammatory response, reducing oxidative stress and apoptosis and promoting tissue repair.

Ischemic damage is the major cause of neuronal death in the central nervous system leading to significant loss of function in millions of individuals each year. As a direct extension of the central nervous system, the retina suffers many of the same hypoxic injuries. Ischemic retinopathies such as those associated with diabetes and prematurity are the leading causes of visual loss in individuals under the age of 55 and neonates, respectively. Vision loss in these individuals occurs as a result of abnormalities in the retinal vasculature, leading to retinal edema, hemorrhage, gliosis (scarring) and/or neovascularization and, in some cases, tractional retinal detachments and blindness. Therapeutic interventions focus on eliminating the vascular abnormalities through the use of lasers or angiostatic drugs injected intravitreally. While dramatic effects can be achieved in select groups of patients, most experience disease progression and associated vision loss.

Stem and progenitor cells have been isolated from bone marrow (BM), peripheral or human umbilical cord blood (hUCB) as an innovative therapy for treatment of ischemic and neuro-degenerative retinopathies. The utility of such a treatment comes from the ability of stem/progenitor cells to differentiate into mature cells and to repair damaged tissue and/or provide direct, paracrine rescue effects. These cells and their differentiated progenies may also recruit endogenous and circulating cells to areas of damaged tissue, contributing to the rescue effect.

UCB is a rich source of hematopoietic stem cells (HSCs) including high numbers of early and late myeloid progenitor cells[1]. Compared to adult BM and peripheral blood, UCB-derived progenitor cells exhibit increased capacity to proliferate and subsequently differentiate into colony forming unit-granulocyte macrophages (CFU-GM)[2]. In addition, UCB-derived cells are less mature relative to adult stem cells; they have not been exposed to immunologic challenge and are unable to activate cytotoxic T-lymphocytes to synthesize pro-inflammatory cytokines[3].

Reports from several groups have shown that local transplantation or intravenously injected UCB-derived mononuclear cells improves functionality in areas of ischemia[1,4] This rescue function is associated with the CD14$^+$ monocyte fraction since depletion of these cells from the UCB led to loss of the rescue function in a rat model of middle cerebral artery occlusion[5]. *In vitro*, the UCB-derived CD14$^+$ cells can differentiate into endothelial[6,7], neuronal[8,9] and mature myeloid (e.g., monocytes, macrophages and dendritic) cells. UCB-derived neural progenitors have also been observed to be neuroprotective in an *in vitro* model of ischemia[10]. Recent

reports suggest that different tissue microenvironments expose myeloid cells to multiple stimuli influencing their fate into pro-, and anti-inflammatory macrophages (M1 and M2, respectively), endothelial, or dendritic cells[11–15]. Thus, different subpopulations of myeloid cells could exert opposite effects during angiogenesis; one population may contribute to plaque formation in experimental models of arterial occlusion[16] where another may promote collateral growth to alleviate ischemia[17]. The retina provides a good model system in which to study these discordant results; tissue-resident and recruited macrophage populations have been implicated in both developmental[18] and pathologic angiogenesis[19], processes that may occur simultaneously in the same tissue during response to ischemic injury.

A recent study[20] has examined the role of macrophages in the establishment of vascular networks. These cells act as "bridge cells" by establishing tip-cell anastomosis and releasing angiogenic factors, such as VEGF, that can lead to vessel fusion and vascular network formation. Previous studies of the same cells have demonstrated that tumours or developing/regenerating tissues can actively recruit these cells from the circulation[21].

In our study we have used hUCB to obtain an enriched population of myeloid progenitor cells, $CD14^+$ cells, which when injected in eyes of mice with oxygen-induced retinopathy (OIR), exerted a profound rescue effect. Only $CD14^+$ cells polarized to M2 macrophages were able to control the pathological neovascularization. In order to better understand the molecular events that regulate the observed rescue effect we: (i); studied the fate of the $CD14^+$ in the retina; (ii) quantified the level of gene expression of injected hUCB-derived $CD14^+$ cells before and after rescue using transcriptomic analysis with human specific primer probes; and (iii) studied the metabolic deregulation occurring in the retinas of OIR mice by mass spectrometry-based metabolomics before and after injection of $CD14^+$ cells. From these studies we conclude that hUCB $CD14^+$ cells differentiate *in vivo* into type 2 macrophages and initiate a series of events associated with modulation of the inflammatory response leading to reduced oxidative stress and apoptosis and, ultimately, promoting normal angiogenesis and tissue repair in the retina.

Our ability to directly image and follow the fate of human monocytes *in vivo*, together with the use of cell/tissue-specific transcriptomic and metabolomic analysis of these cells and their target tissue provide novel insights into the behaviour of monocyte/macrophage cellular subsets during angiogenesis and inflammation.

Results

Human umbilical cord blood-derived $CD14^+$ cells stabilize ischemia-injured vasculature in the retina. In the mouse OIR model, a transient period of hyperoxia during retinal vascular development attenuates normal retinal vessel development and leads to degeneration of the newly formed, immature vasculature. Upon return to normoxia, the central retinal area where the vasculature has regressed becomes hypoxic leading to development of pathological neovascularization (NV) at the interface between perfused and non-perfused retina[22]. In this model, the retinal vasculature of both BALB/cByJ and C57BL/6J strains of mice becomes obliterated to a similar extent. However, in retinas from BALB/cByJ mice, the vaso-obliterated regions revascularize more rapidly and pathological, pre-laminar neovascular tufts do not form. In contrast, the retinas of pigmented C57BL/6J mice are characterized by slower revascularization of the central retina and there is extensive formation of pathological, pre-laminar neovascular tufts (Supplementary Fig 1A).

We also hypothesized retinas in the BALB/cByJ strain is protected from neovascularization by a more rapid recruitment of endogenous anti-inflammatory microglia during the hypoxic phase of the OIR model (unpublished observations).

Freshly isolated $CD14^+$ cells derived from hUCB consist of a heterogeneous population of myeloid cells. The $CD14^+$ cells were injected intravitreally at postnatal day 7 (P7) in C57BL/6J pups and the mice were maintained in an atmosphere of 75% oxygen for 5 days (P7–P12) to induce the ischemic retinopathy. At P17, vaso-obliteration and neovascularization were reduced by 63% and 56%, respectively, in retinas treated with $CD14^+$ cell grafts compared to retinas treated with the vehicle DPBS (Fig 1A, B). No significant rescue effect was observed when $CD14^-$ cells were used (Fig 1B).

Next, $CD14^+$ cells were transduced with an adenoviral vector (Ad5 F16) encoding enhanced-green fluorescent protein (eGFP)[25] to assist in visualizing the cell transplants. The eGFP-labelled $CD14^+$ cells were observed to target the retinal vessels from P12 and to be primarily localized around the retinal vasculature 10 days after intravitreal injection (P17). $CD14^+$ cells targeted the vessels showing highly arborizing processes with a macrophage cell-like shape. $EGFP^+$ cells wrapped around vessels for long distances and when targeting the neovascularization areas maintained a round morphology as fresh isolated from the cord blood (Fig 1C, D, E). Using 3D image reconstruction, we confirmed that the $CD14^+$ cells were localized to the vascular surface and not integrated into the vessel itself. Importantly, intravitreal injection of $CD14^+$ cells infected with Ad5F16-eGFP did not reduce the rescue function observed with a non-Ad5F16-eGFP infected $CD14^+$ cells, indicating that transduction of the cells with the Ad vector does not significantly impact rescue. From these observations we conclude that hUCB-derived $CD14^+$ cells differentiate *in vivo* into a myeloid cell with dendritic-macrophage cell-like morphology, exert trophic rescue effects in the mouse OIR model and do so by adhering to, and wrapping around, the retinal vasculature rather than integrating into it. This rescue effect and differentiation is not an immunological response associated with the injection of human cord blood cells into the mouse eye (xenotransplant); the rescue and differentiation effects were not observed with the injection of human $CD14^-$ cells into the mouse eye (Figure 1B). Next, we conducted a molecular characterization of injected cells and retinal tissue in order to better understand the mechanism by which $CD14^+$ cells promote normalization of retinal vasculature and tissue repair.

hUCB-derived $CD14^+$ cells reduce level of ischemia and stimulate the recruitment of endogenous myeloid cells. Injection of $CD14^+$ cells significantly reduced the area of vaso-obliteration, thus limiting retinal vascular damage and enhancing tissue repair during the period of hyperoxia (P7–P12). We observed a 50% reduction of obliterated area at P12 (one day after returning to normoxia) (Fig 2A) and significant recruitment of lectin positive cells such as leukocytes and EPCs from the peripheral blood when we injected $CD14^+$ cells compared to vehicle injection (Fig 2B, C, D). These cells have been demonstrated to be fundamental not only for an ischemic tissue repair but also for the stabilization of retinal vasculature[26]. It is important to note that in a normoxic environment at P12, formation of the superficial retinal vascular plexus is already complete but the deep and intermediate vasculature is still forming through P21. $CD14^+$ cells, by contributing to the recruitment of angiogenic cells, maintain vascular growth in the deep plexuses and prevent neovascularization formation at P17.

Next, we undertook a human specific transcriptomic analysis of P17 mouse retinas with the injection of hUCB $CD14^+$ and $CD14^-$ cells to define the differentiation state of the human cells and the mechanism of action contributing to their rescue of OIR retinas during hypoxia.

Cord blood-derived $CD14^+$ cells express mRNAs associated with the oxidative stress response, cell cycle, and macrophage cell markers. The molecular changes associated with stabilization of retinal vasculature by hUCB-derived $CD14^+$ cells were assessed at the mRNA level by selectively detecting and quantifying the expression level of 50 human genes in the mouse retina. Specifically, we measured the expression ratio of human genes in the mouse retina at P17 after intravitreal injection at P7 of $CD14^+$, $CD14^-$ cells (control

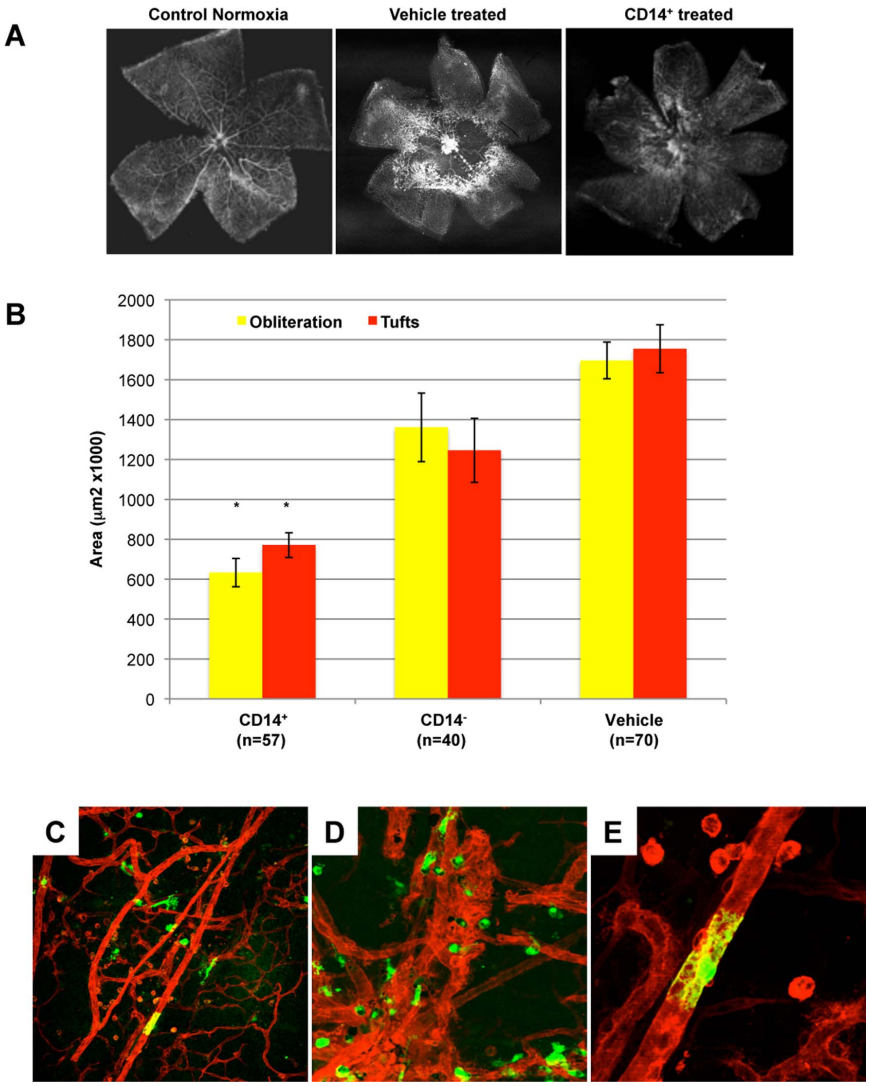

Figure 1 | CD14⁺ cells stabilize and promote normalization of ischemia-injured retinal vasculature in the OIR model. A) CD14⁺ cells normalize angiogenesis during hyperoxia and accelerate retinal revascularization. Normal retinas were dissected from C57BL/6J mice and stained with GS lectin at postnatal day 17 (P17). They show a characteristic branching vascular pattern radiating outward from the central optic nerve head (''Control Normoxia''). Exposure to hyperoxia for 5 days (from P7 to P12) leads to central vaso-obliteration. Once the mice return to normoxia, neovascularisation occurs at the interface between perfused peripheral, and non-perfused central, retina. Treatment with vehicle (''Vehicle treated'') at P7 does not alter the vaso-obliteration or neovascularisation. In contrast, treatment at P7 with hUCB-derived CD14⁺ cells leads to normalization of the retinal vasculature (''CD14⁺ treated''). B) Quantification of retinas treated with hUCB-derived cell populations. Retinas were analyzed at P17 using GS-lectin staining for retinal vessel obliteration (yellow bars) and tuft formation (neovascularization) (red bars) in retinal whole mounts. No significant difference was observed between vehicle and CD14⁻ cells when injected intravitreally at P7. Obliteration and neovascularization are reduced by 63% and 56% respectively, compared to vehicle-treated retinas (n=57, n=40, n=70, n=number of eyes) (*P <0.001 Bonferroni corrected t-test). C) D) And E) Ad5F16-eGFP hUCB-derived CD14⁺ cells (green) target and differentiate along the mouse retina vasculature (red) at P17 (10x, 20x and 40X respectively).

population), or vehicle in the OIR model (Fig 3). Transcriptomic analysis of retinas treated with CD14⁺ cells revealed increased expression of human antigens of M2 macrophages. The molecule CD14 and other monocytic cell markers such as CD163[27], CD68[28], CD209[29] and HLA-DRA[30] were highly upregulated after the injection of CD14⁺ relative to CD14⁻ (CD14⁺/CD14⁻ >1.6). Importantly, we also detected increased expression of human genes (CD14⁺/CD14⁻ >1.6) associated with the oxidative stress response including *SOD1*, encoding superoxide dismutase 1. Interestingly, in freshly isolated cells (day 0) *SOD1* expression was higher in CD14⁻ population compared to CD14⁺ cells (Supplementary Fig 2). Additional oxidative stress-associated genes were also detected including human *CAT, GPX1, HMOX1 and ALDOA*.

The CD14⁺ cells also induced expression of genes (CD14⁺/CD14⁻ >1.6) involved in cell signaling such as IFI16[31], IFI6, BCL2A1, AKT1 and *NF*-κB1. TGF*β1*, expressed by the leukocyte lineage to control cell differentiation, proliferation, and resolution of inflammation, was also highly up regulated in the mouse retina at P17 after injection of CD14⁺ cells. The transcription factor STAT3, responsible for controlling anti-inflammatory pathways[32,33], was up regulated by CD14⁺ cells compared to the negative fraction. We also observed that TNF, a cytokine responsible for the recruitment of pro inflammatory leukocytes, was not expressed by CD14⁺ cells and is, in fact, slightly down regulated compared to the negative fraction.

Genes associated with cell adhesion such as ICAM-1 (also known as CD54), human CD44 and ITGAM were also highly expressed after injection of CD14⁺ cells relative to CD14⁻ and vehicle. Other genes with diverse biological roles were also up regulated by the intravitreal injection of hUCB-derived CD14⁺ cells relative to the CD14⁻ fraction and vehicle: (i) human *CCR5*, encoding CC chemokine receptor

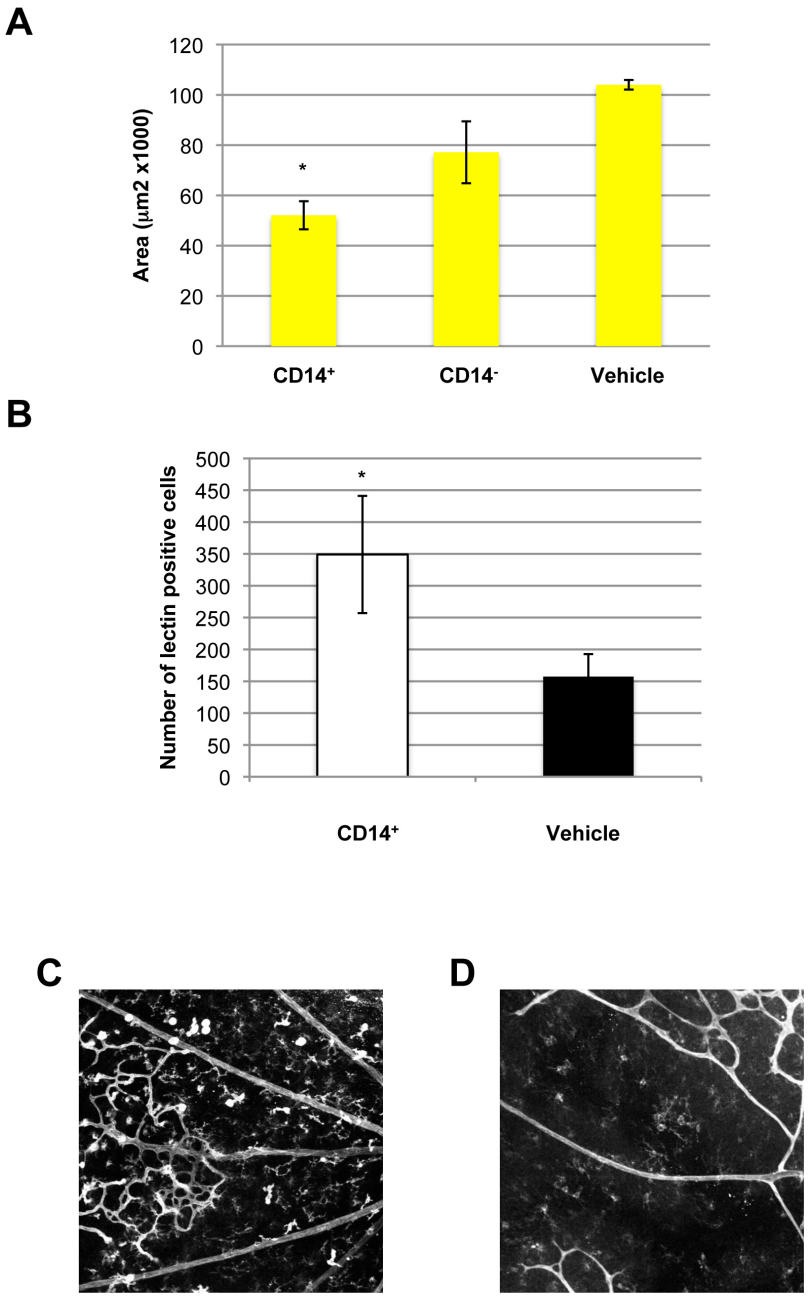

Figure 2 | CD14$^+$ cells promote angiogenesis and recruit endogenous proangiogenic cells in hypoxic areas (A) At P12 the obliteration area in CD14$^+$ treated eyes is reduced by 50% compared to vehicle-treated retinas (n=8, n=number of eyes for each condition). (B) Lectin-positive cells in areas of vaso-obliteration are increased 2.2- fold after intravitreal injection of CD14$^+$ cells relative to vehicle injection (n=6, n=number of eyes for each condition) (*$P<0.001$ Bonferroni corrected t-test). (C) 10x confocal images of retinas treated with CD14$^+$ shows high recruitment of lectin-positive cells with microglial-like morphology. (D) Lectin-positive cells are absent in vehicle-injected retinas.

5, a protein predominantly expressed on T-cells, macrophages, dendritic cells and microglia that binds cytokines as MIP-1alpha and beta and Rantes; (ii) *ALDOA*, encoding aldolase A; (iii) *HIF1A*, hypoxia-inducible factor 1-alpha; (iv) *GUSB*, encoding *β-glucuronidase*; and (v) *SERPINA 1* (also *alpha-1-antitrypsin*), encoding a serine proteinase inhibitor that protects tissues from enzymes of inflammatory cells such as elastase. Interestingly, the tissue inhibitor metalloproteinase 1 (TIMP1), known to inhibit the activity of MMP1 and MMP13 and so to block angiogenesis *in vivo* and *in vitro*[34] was up regulated by the positive fraction compared to the negative population.

Overall, the transcriptomic data supports our initial histological and antibody array results indicating that CD14$^+$ differentiates into a macrophage polarized M2 type and exerts rescue effects in association with the expression of genes that regulate oxidative stress, apoptosis and control of inflammation and angiogenesis.

HUCB-derived CD14$^+$ cells reduce the levels of oxysterols in OIR retinas, resembling the response of BALB/cByJ mice to hypoxia. Severe levels of oxidative stress can damage all components of the cell, including metabolic intermediates such lipids (i.e., lipid peroxidation). Therefore, we performed a metabolomic analysis using mass spectrometry in order to investigate whether the rescue effects of the CD14$^+$ cells are partially explained by their capacity to suppress metabolic oxidative damage in retinal tissue.

We analyzed retinas of C57BL/6J mice at P12 as the first stage between the hyperoxia and hypoxia, P15 as middle hypoxia and P18

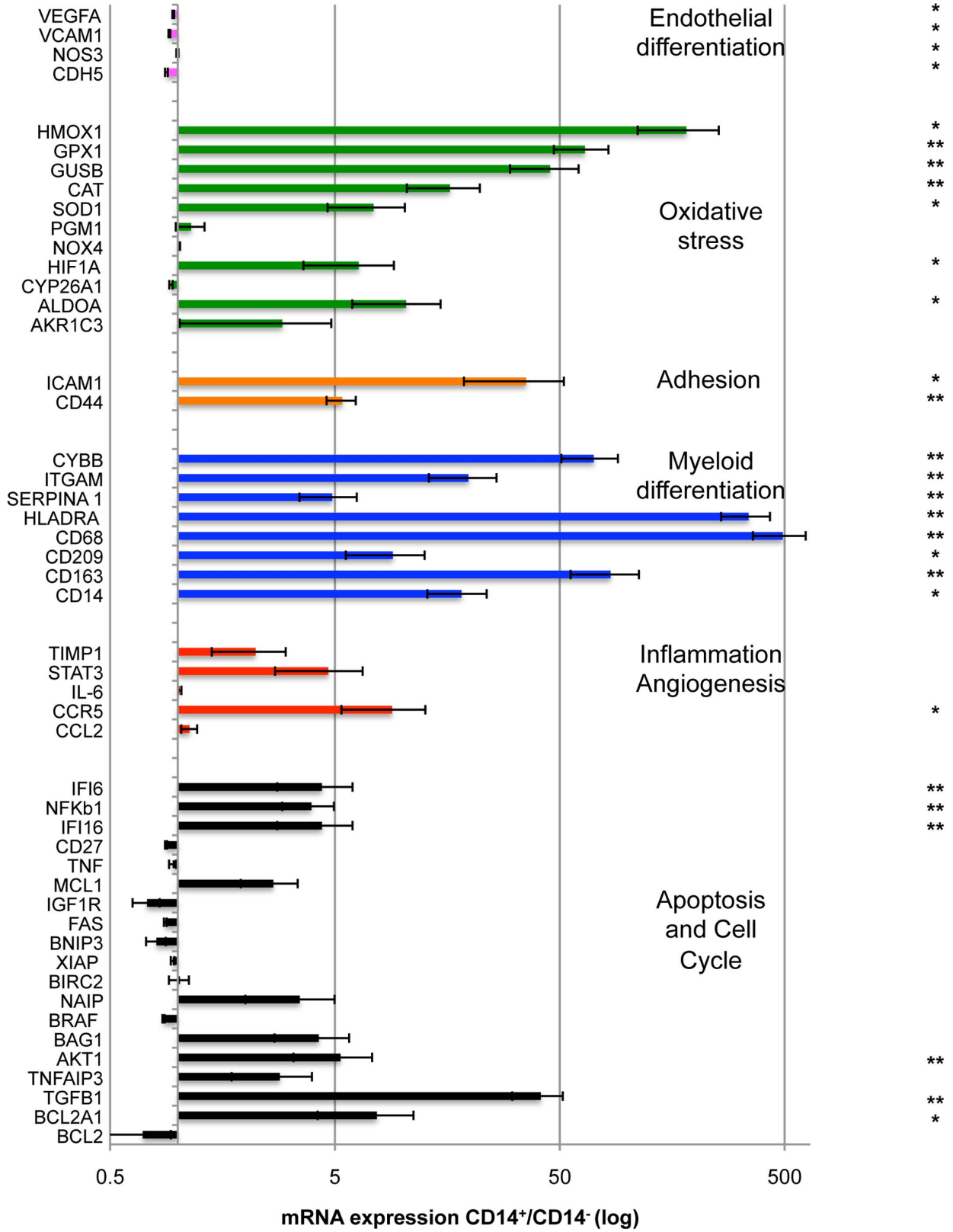

Figure 3 | Human UCB-derived CD14$^+$ cells regulate oxidative stress and apoptosis, and express markers of myeloid cell differentiation in the OIR model. Several human genes are up-regulated at P17 in the CD14$^+$-treated retinas compared to retinas injected with the negative fraction, CD14$^-$ cells and compared to retinas injected with the vehicle, DPBS. A fold increase of 1.6 or greater of anti-apoptotic genes is observed (black) (IFI6, IFI16, AKT1, BCL2A1). Human anti-oxidative stress genes are significantly up regulated when CD14$^+$ cells are injected compared to the negative fraction (green). Numerous genes characteristic of myeloid cell differentiation are highly expressed in the CD14$^+$-treated retinas (blue). The CD14$^+$ cells increase expression of vascular adhesion molecules (ICAM1) and the extracellular matrix receptor (CD44) (orange). Genes characteristic of endothelial cell differentiation (VEGF) and inflammation (TNF, IL6) are not significantly different between the CD14$^+$ cells and the retinas treated with the negative fraction. (n=12, n=number of retinas independently extracted and analyzed for each treatment) (*P <0.01; **P <0.001).

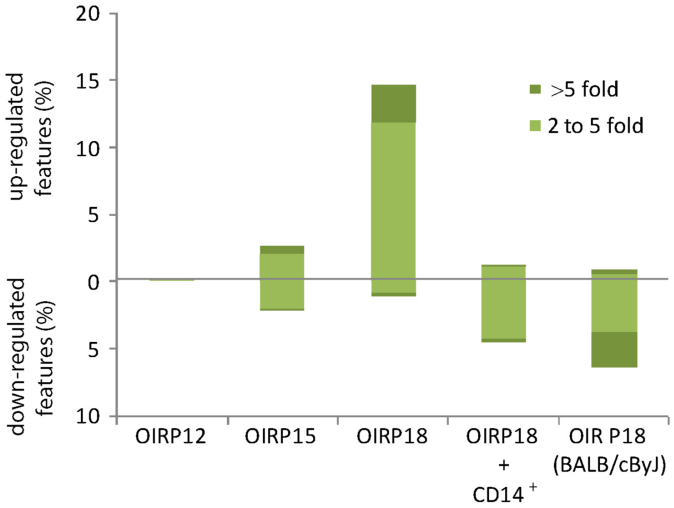

Figure 4 | Global metabolomic analysis of the OIR model. Bars indicate the percentage of up-regulated or down-regulated mass spectrometry features (*P <0.01) in the OIR retinas relative to normoxia at post natal day 12, 15 and 18. Results correspond to C57BL/6J mouse strain unless otherwise stated. 8–12 independently extracted retinal tissues were analyzed for each time point or treatment, n=8–12).

as advanced hypoxia and compared metabolite levels between normoxia and OIR, and between retinas treated with $CD14^+$ cells and vehicle. Untargeted metabolomic analysis (Fig 4) revealed only minor changes between normoxia and OIR at P12, indicating that hyperoxia does not significantly affect the metabolome in the developing retina. By P15, (after 3 days of induced-hypoxic conditions) only ~4% of the metabolites detected were up regulated (>2 fold; P <0.01) in OIR retinas relative to normoxia. However, after 6 days under hypoxic conditions (P18), and coinciding with the observed histopathological changes (i.e. neovascular tufts) observed in the OIR model, approximately 15% of the metabolites detected in OIR retinas were differentially regulated (>2-fold, P <0.01) relative to normoxia. In contrast, when the retinas were treated with $CD14^+$ cells at P7, only ~2% of the metabolites remained deregulated (>2-fold, P <0.01) at P18 (Fig 4). We used tandem mass spectrometry (i.e. ESI-Q-TOF MS) to identify of some of the metabolites deregulated at P18 under OIR conditions whose levels were normalized by intravitreal injection of $CD14^+$ cells. The deregulated metabolites included oxysterols such as 5,6β-epoxy-cholesterol, 7-ketocholesterol, and 7α-hydroxycholesterol (Table 1). Oxysterols are oxidation products of cholesterol that exert cytotoxic, pro-oxidant and pro-inflammatory effects *in vivo*[35–38]. We also observed the accumulation of several acyl-carnitine structures at P18 in OIR retinas. Acyl-carnitines are fatty acyl-CoA (coenzyme A) conjugated to carnitine and assist with the transport and metabolism of fatty acids into mitochondria, where they are undergo β-oxidation. Importantly, 11-cis-retinal was identified as one of the few metabolites whose abundance decreased at P18 in the OIR model. The metabolite 11-cis-retinal is an endogenous chromophore bound to opsin; its photoisomerization is the chemical basis for vertebrate vision. The level of oxysterols (Supplementary Fig 3A,B,C) and 11-cis-retinal (Supplementary Fig 3D) was completely normalized at P18 by the treatment with $CD14^+$ cells and the level of acyl-carnitines was significantly reduced (~2-fold) compared to the non-treated retinas (5–9 fold) (Table 1).

Previous studies have shown that BALB/cByJ mice placed into the OIR model do not form tufts to an appreciable degree and the central vaso-obliteration area revascularizes quickly following return to normoxia[26]. When untreated, wild type BALB/cByJ mouse retinas were analyzed at P18 under the OIR conditions using the same untargeted mass spectrometry-based metabolomic approach, we observed a global trend similar to that observed in C57BL/6J mice treated with $CD14^+$ cells under OIR conditions (Fig 4). Essentially, only ~1.7% of the metabolites detected in BALB/cByJ retinas appeared up regulated (> 2-fold, P <0.01) at P18 relative to normoxia. It is of interest to note, however, that both BALB/cByJ and C57BL/6J mice treated with $CD14^+$ cells showed a markedly high percentage of down-regulated metabolites relative to normoxia at P18.

Overall, the metabolomic data reveals that oxidative damage in the retina does not occur during the period of hyperoxia, but does so as the result of the oxygen/reperfusion injury following the induced-hypoxia. Importantly, our results also demonstrate that intravitreal injection of $CD14^+$ cells reduces the metabolic oxidative damage by controlling the production of oxysterols.

5,6β-epoxy-cholesterol and 7-ketocholesterol induce astrocyte disorganization, gliosis, and apoptosis by activating caspase 3. Having observed a high expression level of genes that regulate apoptosis in retinas treated with $CD14^+$ cells, we studied the role of oxidized forms of cholesterol in the pathogenesis of retinal tissue. Initially, astrocytes and endothelial cells, two different cell types found in the retina, were cultured *in vitro* and treated with the identified oxysterols in a dose-dependent manner. Cultured mouse astrocytes exhibited a dose-dependent toxicity response after treatment with increasing concentrations of β-epoxy-, 7α-hydroxy-, and 7-ketocholesterol (Supplementary Fig 4A). At the highest dose tested, 0% (P <0.001) and 4.8 ± 4.5% (P <0.001) of the astrocytes were viable after treatment with 7-keto- and β-epoxycholesterol, respectively, compared to 80 ± 4.5% viability in the astrocyte culture treated with vehicle (i.e., regular media and

Table 1 | Fold change of oxysterols, carnitines and 11-cis retinal in OIR retinas compared to Normoxia

	C57BL/6J (P18)				BALB/cByJ (P18)	
	OIR/Normoxia		OIR+$CD14^+$/ Normoxia		OIR/Normoxia	
Metabolite	Fold	P value	Fold	P value	Fold	P value
7-ketocholesterol	6.7	2.3×10^{-6}	1.3	0.2	1	0.67
5,6β-epoxy-cholesterol	5.1	2.1×10^{-6}	1.4	0.37	1.1	0.78
7α-hydroxycholesterol	3.9	5.8×10^{-6}	1	0.91	1	0.68
11-cis-retinal	0.3	5.6×10^{-5}	0.83	0.047	n.d	n.d
Decanoylcarnitine	5.7	9.0×10^{-8}	2	0.002	2.4	4.2×10^{-6}
Octanoylcarnitine	5.5	5.5×10^{-4}	2.2	9.58×10^{-5}	1.8	5.4×10^{-5}
Laurylcarnitine	9.1	2.9×10^{-7}	2.6	7.8×10^{-4}	2	1.0×10^{-5}
Tetradecenoylcarnitine	8.8	7.5×10^{-9}	2.1	1.1×10^{-4}	1.2	0.02
Hexadecenoyl carnitine	5	3.1×10^{-9}	1.3	0.032	0.6	0.016
Tetradecanoylcarnitine	7.2	5.9×10^{-9}	2	2.9×10^{-4}	1.4	0.0013

ethanol) (Supplementary Fig 4B). In the presence of 7α-hydroxycholesterol, cell viability was 63.1 ± 3.9% ($P > 0.05$). Alternatively, when cultured human vascular endothelial cells (HUVEC) were exposed overnight to 40 μg/ml of 5,6β-epoxy-cholesterol, only 4.6% of the cells remained viable ($P < 0.001$) (Supplementary Fig 4C). The alpha isomer (5,6α-epoxy-cholesterol), however, maintained HUVEC viability close to 60% (data not shown), indicating the functional specificity of this metabolite. HUVEC were exposed to hydrogen peroxide (H_2O_2) as a positive control of cellular toxicity (Supplementary Fig 4C).

To better understand the mechanism by which these oxidized forms of cholesterol were toxic, we studied the cleavage of caspase-3, a marker of apoptosis. Using Western blot analysis, we observed activation of caspase-3 in cell cultures of bovine aortic endothelial cells (Fig 5A) or mouse astrocytes (Fig 5B) treated with 5,6β-epoxy-, 7-keto-, and 7α-hydroxycholesterol. This is consistent with the

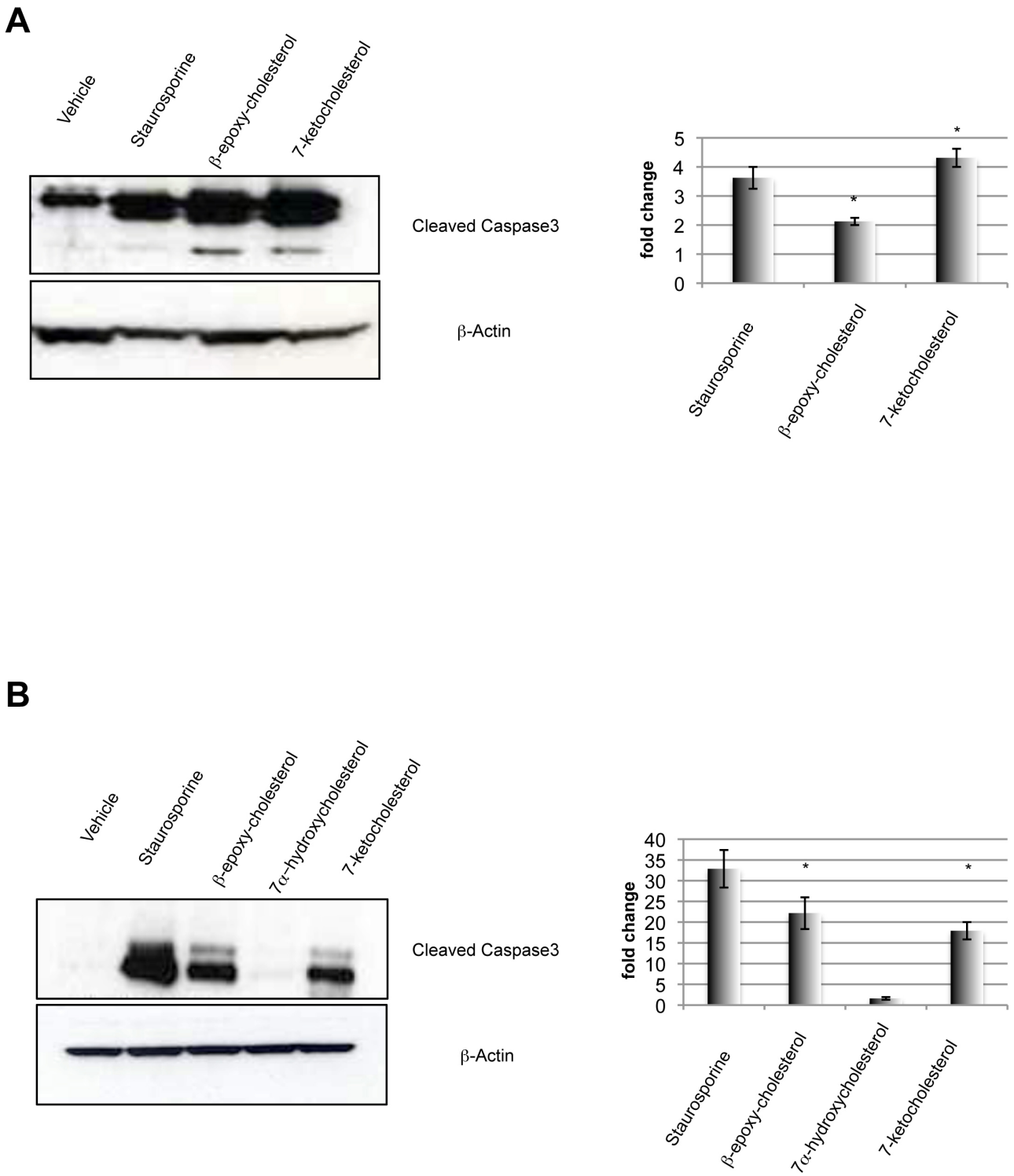

Figure 5 | Oxysterols induce apoptosis in endothelial cells and astrocytes *in vitro*. Western Blot analysis shows the cleavage of Caspase-3 induced by β−epoxycholesterol and 7-ketocholesterol in Bovine Aortic Endothelial cells (A) and C8-D1A astrocytes (B). Staurosporin (ST) was used as positive control. Actin level is reported to normalize the quantity of protein in each sample (n=3, n=number of experiments) (Bonferroni corrected t-test: $*P < 0.01$).

increased activation of caspase-3 cleavage in whole retinas obtained from mice under OIR conditions. We observed an increase of 65% and 130% of caspase-3 cleavage in OIR retinas at P15 and P18, respectively, relative to normal developing retinas (Supplementary Fig 5). No observable difference in caspase-3 cleavage was observed at P12 between normal and OIR retinas (data not shown).

The morphological effect of intravitreally injecting β-epoxy-, and 7-ketocholesterol into P15 mice under normal developing conditions (i.e. normoxia) was evaluated 3 days later after treatment (P18). Compared to control eyes (Fig 6A, a), retinas injected with 5,6 β-epoxy- (Fig 6B, b) or 7-ketocholesterol (Fig 6C, c) showed disruption of the astrocytes associated with the superficial retinal vascular plexus and a strong

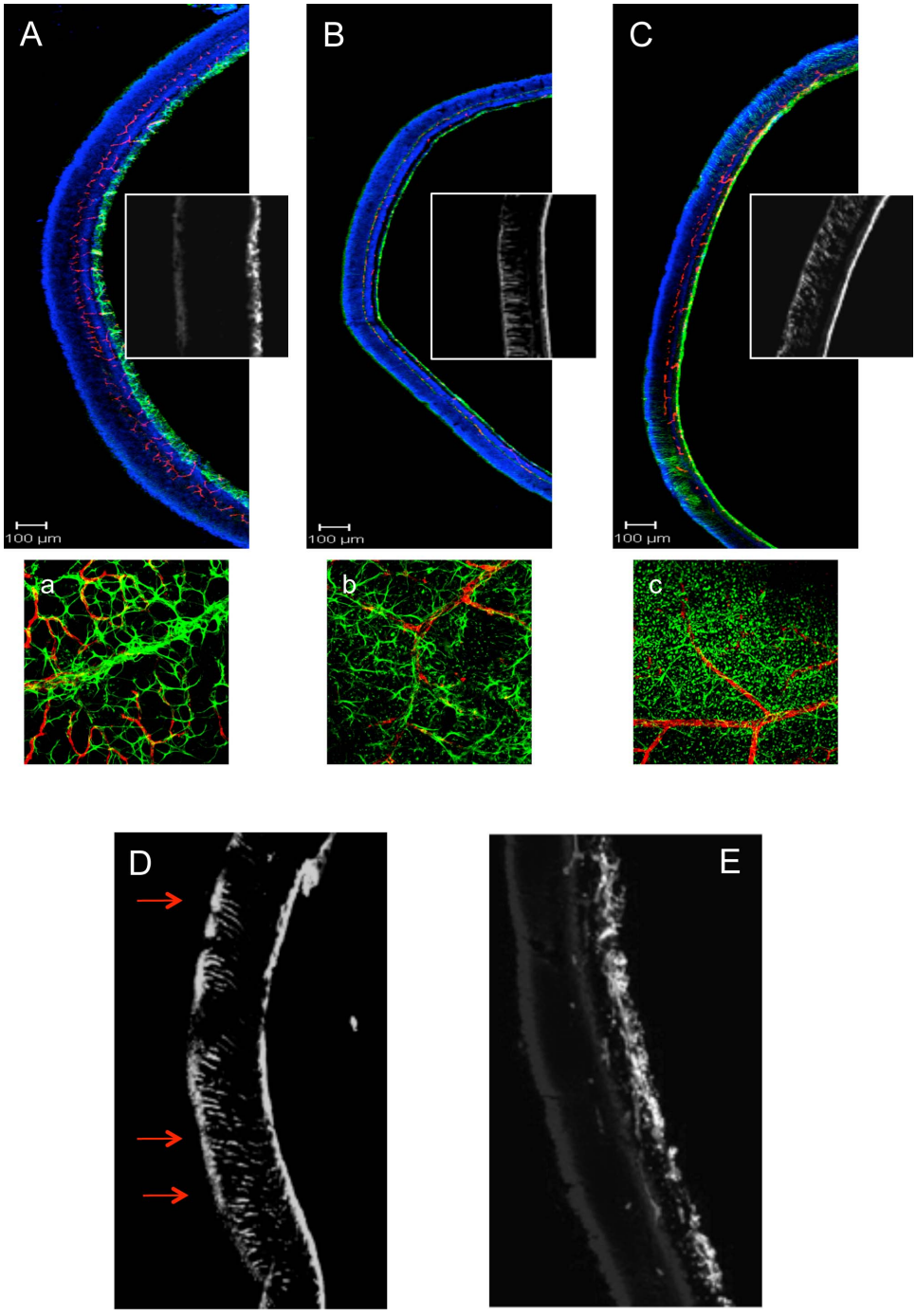

Figure 6 | Oxysterols are toxic for astrocytes and muller glia cells *in vivo*. Immunohistochemical analysis using lectin (red, blood vessels) and antibody to GFAP (green, astrocytes and activated Muller glia cells) demonstrates the normal retina (A) or abnormalities observed with degeneration of astrocytes in the inner retina after intravitreal injection of β-epoxy-cholesterol (B) or 7-ketocholesterol (C). Insets in A, B and C represent 20X magnification views of GFAP expression. Inset figures a, b, c show 20X magnification views of whole mount retinas from the same specimen; astrocytes (green) appear damaged and the muller glia cells (green dots) are visible in the superficial plexus of the vasculature (red) demonstrating severe gliosis (n=5, n=number of eyes for each treatment). **HUCB derived CD14$^+$ cells prevent Muller Glia cells activation in OIR retinas.** Immunohistochemical analysis using an antibody to GFAP demonstrates degeneration of astrocytes layer and gliosis (red arrows) in P17 OIR retinas (D). Treatment with HUCB CD14$^+$ cells prevents this damage (E) (n=6, n=number eyes for each condition).

activation of Muller glia cells in the outer layer. Similarly, retinas from OIR mice (not exposed to exogenous 5,6 β-epoxy-, and 7-ketocholesterol) showed reactive gliosis of the muller glia cells at P18 (Fig 6D). The treatment of OIR retinas with $CD14^+$ cells prevented disorganization of the astrocytic layer and reactive gliosis (Fig 6E).

Overall, our results indicate that accumulation of β-epoxy- and 7-ketocholesterol metabolites in the OIR retinas induces apoptosis by activation of caspase-3 cleavage, leading to a disruption of the astrocyte organization and gliosis of the Muller glia cells in the outer layer. Treatment with $CD14^+$ cells restores the phenotype to that of normal developing retinas.

Polarized M2 macrophages derived from $CD14^+$ cells prevent neovascularization in ischemic retina. The molecular characterization of the rescue effects observed in OIR retinas treated with $CD14^+$ cells showed a high degree of myeloid macrophage differentiation and recruitment of lectin-positive cells. We hypothesized that polarized activation of macrophages may be the primarily mediator of the rescue effects in the OIR model. To test this hypothesis, we induced the *in vitro* differentiation of freshly isolated human UCB-derived $CD14^+$ cells into activated M1 and M2 macrophages, and each population of activated macrophages was then injected intravitreally in OIR mice.

IFN-γ alone, or in concert with microbial stimuli or cytokines, has been known to induce differentiation of monocytes into activated M1[39]. M2 is a generic name for various forms of activated macrophages, excluding M1 cells but including cells exposed to IL-4 or IL-13, immune complexes, IL-10, glucocorticoids, or vitamin D3-derived metabolites[40]. M1 macrophages were obtained by *in vitro* differentiation of $CD14^+$ cells using IFN-γ, and M2 macrophages were obtained using IL-4 as previously described[41,42]. After 3 days of *in vitro* differentiation, we used flow cytometry to assess the level of pro- and anti-inflammatory cytokines secreted by M1 and M2 subsets. IFN-γ-stimulated $CD14^+$ cells secreted high levels of pro-inflammatory cytokines IL-8, IL1β and IL-6, whereas IL-4-stimulated $CD14^+$ cells secreted high levels of anti-inflammatory IL-10 (Supplementary Fig 6).

Three days after *in vitro* differentiation, M1 and M2 populations derived from $CD14^+$ cells were injected intravitreally at P7, and the mice were maintained in an atmosphere of 75% oxygen for 5 days (P7–P12) to induce ischemic retinopathy. The areas of vaso-obliteration measured at P17 were reduced by 75% and 96% in retinas treated with M1 and M2 grafts, respectively, compared to the vehicle DPBS (Fig 7A, yellow bars). Importantly, only the M2 population prevented tuft formation (i.e. neovascularisation) showing a reduction of 59% of neovascular areas (Fig 7A, red bars). We did not observe a significant decrease of tuft formation by activated M1 macrophages. Both populations were able to induce rapid resolution of obliterated areas during the hyperoxic phase, but only the M2 population prevented neovascularization. Thus, the decrease in retinal neovascularization observed in association with reduction of obliteration is not simply a result of a decrease in the vascularized area; both M1 and M2 macrophages reduced obliteration, but only the M2 macrophages also reduced neovascularization. In addition, only M2 grafts induced a massive recruitment of endogenous Mannose Receptor-positive cells, a cell shown by others to control inflammation processes (Fig 7B, C)[43,44].

These data support the concept that this subset of macrophages is predominantly responsible for the rescue effects of hUCB-derived $CD14^+$ cells, either by recruitment of endogenous populations of M2 macrophages and/or by differentiation of $CD14^+$ cells in the ischemic retinas.

Discussion

In this study we demonstrate that hUCB-derived $CD14^+$ myeloid progenitor cells, when injected into the ischemic neonatal eye, will differentiate into macrophage-like cells. The $CD14^+$ cells, once differentiated in mature myeloid cells, recruit and activate endogenous pro-angiogenic cells that facilitate functional angiogenesis and reduce inflammation ordinarily observed during OIR. When we analyzed and compared the transcriptomic profile of $CD14^+$ and $CD14^-$ populations, we observed a different response of the two fractions to the retinal environment. As freshly isolated cells, the two populations exhibit differential expression for many of the genes analyzed while some of the genes exhibit very similar levels of expression.

We have previously demonstrated that BM-derived hematopoietic progenitor cells injected intravitreally will target activated glia, differentiate into endothelial cells and exert trophic rescue activity in animal models of ischemic and neuro-degenerative retinopathies[45,46]. Injection of BM-derived $CD44^{hi}$ cells into hypoxic eyes showed that these cells differentiate into microglia and exert a paracrine-rescue effect, stabilizing damaged retinal vasculature[26]. While heat shock proteins and chaperones were observed to be upregulated in rescued retinal neurons, the precise mechanism of rescue remains unclear. Transcriptomic analysis of $CD14^+$ cells after injection into OIR retinas shows a selective up-regulation of genes associated with M2-polarized macrophages.

Our data suggest that the trophic rescue effect of the $CD14^+$ cells was associated with their differentiation into M2 cells as well as an influx of similar cells from the host circulation. Interestingly, four genes that are expressed at very similar levels between the two cell populations at day 0, show significantly increased expression in the $CD14^+$ retinal transplant including, TGFB1, CAT, GUSB and SOD1. These genes encode proteins with multiple functions including regulation of proliferation, differentiation, adhesion, migration and response to oxidative stress. For example, SOD1 is expressed at lower levels in fresh isolated $CD14^+$ cells compared to $CD14^-$, but in $CD14^+$ transplanted retinas, the expression of this gene was increased significantly compared to $CD14^-$ transplanted retinas.

We hypothesized that the $CD14^+$ fraction can respond to micro-environmental cues and regulates inflammatory cascades as well as the response to hypoxia. During the hyperoxic phase of the OIR model, the $CD14^+$ cells induce angiogenesis, reducing the area of vaso-obliteration and associated tissue hypoxia. Vascular regression, associated with endothelial cell death, is avoided by $CD14^+$ cell-induced up-regulation of anti apoptotic and anti-oxidative genes and associated maintenance of retinal vasculature. Thus, the $CD14^+$ cells differentiate into type 2 macrophages, acquiring an anti-inflammatory phenotype. Recent studies have shown that tissue macrophages exist as two polarized populations, M1 and M2 subsets[47,48], the former being pro-inflammatory and the latter being anti-inflammatory. The relative immunological immaturity of the UCB-derived cells could explain why most monocyte populations from neonatal blood become M2 polarized cells instead of the pro-inflammatory M1[29]. The M2 cells modulate the inflammatory response and facilitate tissue repair[49] enhancing trophic rescue, enhanced removal of apoptotic cellular debris and inducing tolerance rather autoimmunity[50]. This idea is further supported by our observation that after intravitreal injection of $CD14^+$ cells stimulated to differentiate along M1 or M2 pathways, only the M2 fraction facilitated normalization of the retinal vasculature and decrease pathological neovascularization.

The concept that macrophages play a critical role during pathological angiogenesis is strongly supported by recent work[20] highlighting the role of M2 mouse macrophages (Angiopoietin receptor 1 and Neuropilin1 positive) at the time of brain vascularization. In this study M2 macrophages interact with endothelial tip cells to promote vascular anastomosis downstream of VEGF mediated tip cell formation and sprout induction.

To better understand the molecular events that promote the trophic rescue effects of the $CD14^+$ cells *in vivo*, we also performed

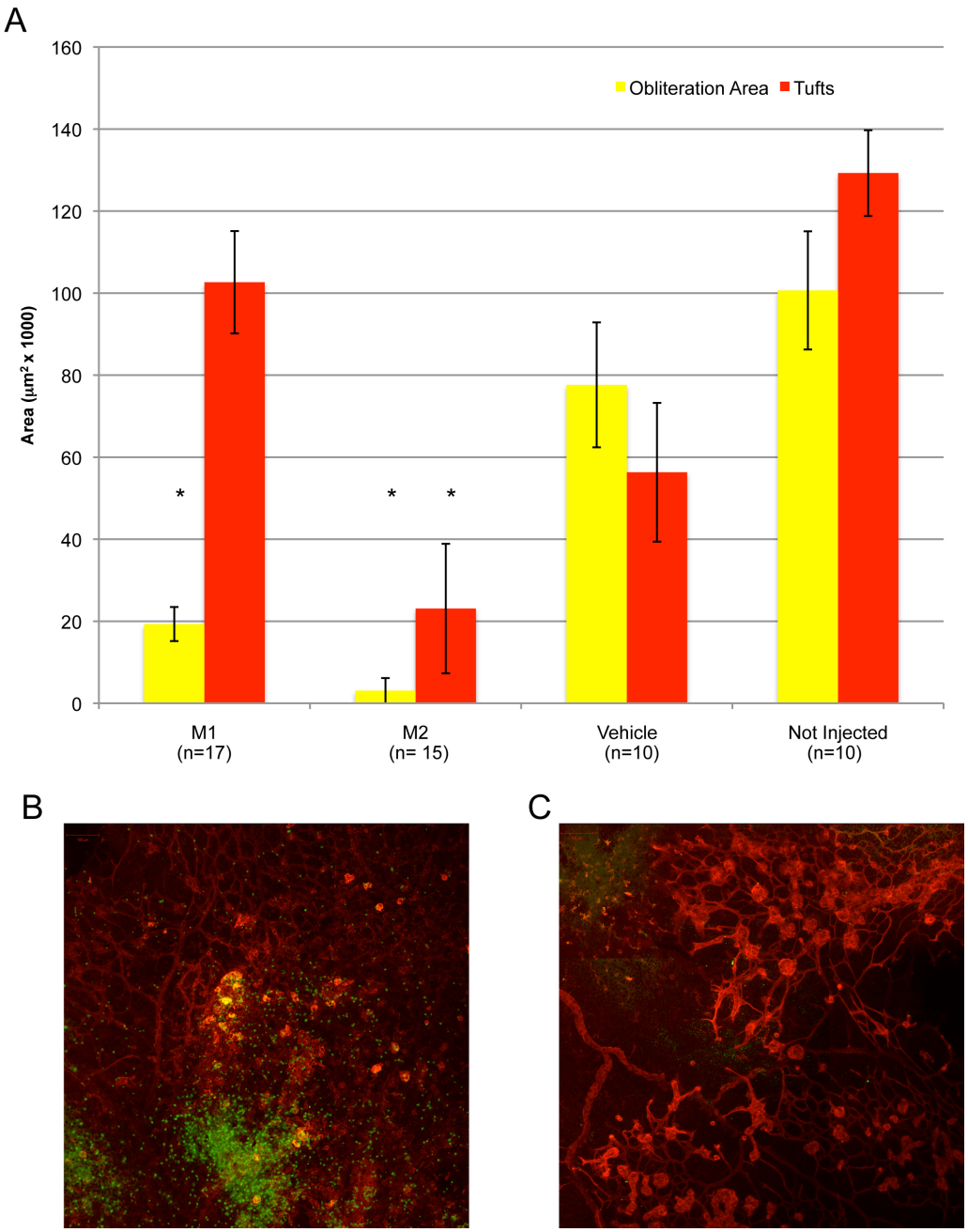

Figure 7 | Intravitreal injection of M2 macrophages derived from CD14$^+$ cells reduces oxygen induced neovascularization. CD14$^+$ cells were differentiated into M1 or M2 cells and injected into the vitreous of P7 mice just prior to high oxygen exposure in the OIR model. At P17 the areas of obliteration (yellow) and neovascular tuft formation (red) were quantified as described in the experimental procedures. Both M1 and M2 populations significantly reduce the areas of obliteration compared to the control-treated eyes (n=17, 15, 10 and 10 respectively, n=number of eyes for each treatment) (Bonferroni corrected t-test, *$P<0.001$). M2 cells are significantly more effective than the M1 cells at reducing the area of neovascularisation compared to the vehicle- or non-injected eyes. (B) At P17, CD14$^+$-treated retinas show recruitment of mouse macrophages expressing mannose receptor (MR) (green). GS-lectin staining shows mouse vasculature (red). (C) MR positive cells are not observed in vehicle-treated eyes (20X).

a comprehensive mass spectrometry-based untargeted metabolomic analysis on normal retinas, OIR retinas and OIR eyes treated with CD14$^+$ cell grafts. A comparison between BALB/cByJ and C57Bl/6J mouse strains was also performed to identify the metabolic features associated with the different behavioral response to the hypoxic conditions characteristic of the OIR model in these two strains. Different oxidized metabolites of cholesterol (oxysterols) were found to be cytotoxic and induce apoptosis in the retinal vasculature and astrocytes. Our results demonstrate that treatment with CD14$^+$ cells controls the deregulation of these metabolites in OIR retinas reducing their toxicity, protecting photoreceptors, glial components of the retina and stabilizing the vasculature.

The use of human umbilical cord blood myeloid progenitor cell-derived monocytes and macrophages represents a promising alternative to adult or embryonic stem cell transplantation for treatment of ocular diseases. These cells have the capacity to promote physiological angiogenesis and to reduce inflammatory processes associated with hypoxic damage in the retina as well as to provide neurotrophic and anti-apoptotic protection to retinal neurons subjected to ischemic damage. In neonates, UCB would be superior to

bone marrow-derived progenitor cells due to the ease of obtaining cord blood at birth and the biological advantages discussed above. The potential utility of these cells in treating ischemic retinopathies such as retinopathy of prematurity and diabetic retinopathy warrants further study.

Methods

Animals and OIR model. All the experiments were performed in accordance with the NIH Guide for the Care and Use of Laboratory Animals and all experimental procedures were approved by The Scripps Research Institute Animal Care and Use Committee. OIR was induced in C57BL/6J mice according to the protocol previously described[22,23]. In some studies BALB/cByJ mice were also subjected to the same conditions.

Cell preparation and characterization. Human cord blood was obtained from National Disease Research Interchange (NDRI). Mononuclear cells were isolated using density gradient centrifugation with Ficoll Paque (Amersham). To isolate the $CD14^+$ fraction human Cord Blood Mono Nuclear Cells (CBMNCs) were incubated with beads attached to anti human CD14 (Miltenyi) and purified according to the MACS separation system protocol provided by the manufacturer.

In vitro infection and labelling of $CD14^+$. Freshly isolated $CD14^+$ cells from human cord blood were incubated for 4–6 hr in M199 medium (Invitrogen) and 20% FBS with Ad5.F16-GFP at an MOI of 5000. After infection the cells were washed from the virus and plated overnight. The percentage of GFP-expressing cells was determined by flow cytometry. For some experiments $CD14^+$ cells were labelled before injection with the Dil (Vybrant dye; InVitrogen) according to the manufacturer's instructions.

Intravitreal injection. Human Cells (250,000/ 0,5 μl) were injected intravitreally using a 33-gauge needle (Hamilton Co.). In the contralateral eye an equal number/ volume of control cells or vehicle alone was injected in Dulbecco's PBS.

Staining and quantification of retinal vasculature.. Retinas were harvested and at various time points for imaging of the vasculature and to localize and characterize endogenous and injected human cells. Quantification of obliteration and neovascularization is described in supplemental information.

In Vitro Differentiation of M1 and M2. $CD14^+$ cells were grown for 4 days in Myco's medium plus 10% of FBS and non-essential aminoacids (NEAN). The M1 population was obtained by adding 1000 U/ml human recombinant IFN-γ (Sigma). M2 cells were obtained using 300 U/ml of human recombinant IL-4 (Millipore). Level of cytokines secreted was measured as described in supplemental information.

Quantitative PCR (QPCR) Gene Expression Analysis. RNA isolation, cDNA synthesis, and real-time PCR analyses were performed as described in Supplemental information.

Metabolite extraction and mass spectrometry analysis. Metabolites were extracted and analyzed by mass spectrometry as previously described[24]. However details are provided in the supplementary information.

Metabolite treatment and Western Blot analysis of cleaved Caspase 3. Mouse astrocytic (C8D1A), human umbilical vein endothelial (HUVEC) and bovine aortic endothelial cells (BAEC) were grown until confluent and treated overnight with different metabolites. Cell death was evaluated by counting the number of trypan blue positive cells. To test the response to metabolites, C8D1A cells were treated overnight with 10 μg/ml, 20 μg/ml, or 40 μg/ml of 5,6β-epoxy-, 7-keto-, and 7α-hydroxycholesterol. 1 mM of H_2O_2 was used as positive control.

For Western Blot analysis, cells and mouse whole retinal lysates were obtained from normal (NOX) and oxygen treated (OIR) retinas at p12, p15, and p18 using lysing buffer (1% Triton X-100, Roche protease inhibitor and 1 mM Sigma phenylmethanesulphonylfluoride). 30 μg of proteins were loaded in each lane and antibody to Cleaved Caspase 3 was used (Cell Signaling). Actin levels were used to normalize the quantity of proteins.

Intravitreal injection of β−epoxy and 7-keto-cholesterol. 0.5 μg and 2 μg of 7-keto-cholesterol and β-epoxycholesterol, respectively, were injected intravitreally at p15. After 3 days, retinas were dissected and stained for glial fibrillary acidic protein (GFAP) and GS lectin. Cryosections were obtained from the same retinas and from OIR P18 retinas treated with vehicle or $CD14^+$ cells. Images were acquired by confocal microscopy using a 20X objective lens. DAPI was used to visualize nuclei.

Data Analysis. Results shown are mean ± SEM. Asterisks signs identify experimental groups that were significantly different from control groups by a t test, one-way ANOVA, with a Bonferroni correction for multiple comparisons where applicable.

1. Newcomb, J. D., Sanberg, P. R., Klasko, S. K. & Willing, A. E. Umbilical cord blood research: current and future perspectives. *Cell Transplant* **16**, 151–158 (2007).
2. Broxmeyer, H. E. *et al.* Growth characteristics and expansion of human umbilical cord blood and estimation of its potential for transplantation in adults. *Proc Natl Acad Sci U S A* **89**, 4109–4113 (1992).
3. Roncarolo, M. G., Bigler, M., Ciuti, E., Martino, S. & Tovo, P. A. Immune responses by cord blood cells. *Blood Cells* **20**, 573–585; discussion 585–576 (1994).
4. Henning, R. J. *et al.* Human cord blood cells and myocardial infarction: effect of dose and route of administration on infarct size. *Cell Transplant* **16**, 907–917 (2007).
5. Womble, T. A., Green, S., Sanberg, P. R., Pennypacker, K. R. & Willing, A. E. CD14(+) human umbilical cord blood cells are essential for neurological recovery following MCAO. *Cell Transplantation* **17**, 485–486 (2008).
6. Kuwana, M. *et al.* Endothelial differentiation potential of human monocyte-derived multipotential cells. *Stem Cells* **24**, 2733–2743 (2006).
7. Romagnani, P. *et al.* CD14+CD34low cells with stem cell phenotypic and functional features are the major source of circulating endothelial progenitors. *Circ Res* **97**, 314–322 (2005).
8. Kodama, H. *et al.* Neurogenic potential of progenitors derived from human circulating CD14+ monocytes. *Immunol Cell Biol* **84**, 209–217 (2006).
9. Chua, S. J. *et al.* Neural progenitors, neurons and oligodendrocytes from human umbilical cord blood cells in a serum-free, feeder-free cell culture. *Biochem Biophys Res Commun* **379**, 217–221 (2009).
10. Arien-Zakay, H. *et al.* Neuroprotection by cord blood neural progenitors involves antioxidants, neurotrophic and angiogenic factors. *Exp Neurol* **216**, 83–94 (2009).
11. Muller, W. A. & Randolph, G. J. Migration of leukocytes across endothelium and beyond: molecules involved in the transmigration and fate of monocytes. *J Leukoc Biol* **66**, 698–704 (1999).
12. Tacke, F. & Randolph, G. J. Migratory fate and differentiation of blood monocyte subsets. *Immunobiology* **211**, 609–618 (2006).
13. Sanberg, P. R. *et al.* Monocyte Transplantation for Neural and Cardiovascular Ischemia Repair. *J Cell Mol Med*, 1582–4934 (2009).
14. Park, D. H. *et al.* Human umbilical cord blood cell grafts for brain ischemia. *Cell Transplant* **18**, 985–998 (2009).
15. Stout, R. D. *et al.* Macrophages sequentially change their functional phenotype in response to changes in microenvironmental influences. *J Immunol* **175**, 342–349 (2005).
16. Luttun, A. *et al.* Revascularization of ischemic tissues by PlGF treatment, and inhibition of tumor angiogenesis, arthritis and atherosclerosis by anti-Flt1. *Nat Med* **8**, 831–840 (2002).
17. Heil, M. *et al.* Blood monocyte concentration is critical for enhancement of collateral artery growth. *Am J Physiol Heart Circ Physiol* **283**, H2411–2419 (2002).
18. Checchin, D., Sennlaub, F., Levavasseur, E., Leduc, M. & Chemtob, S. Potential role of microglia in retinal blood vessel formation. *Invest Ophthalmol Vis Sci* **47**, 3595–3602 (2006).
19. Sakurai, E., Anand, A., Ambati, B. K., van Rooijen, N. & Ambati, J. Macrophage depletion inhibits experimental choroidal neovascularization. *Invest Ophthalmol Vis Sci* **44**, 3578–3585 (2003).
20. Fantin, A. *et al.* Tissue macrophages act as cellular chaperones for vascular anastomosis downstream of VEGF-mediated endothelial tip cell induction. *Blood* **116**, 829–840 (2010).
21. Pucci, F. *et al.* A distinguishing gene signature shared by tumor-infiltrating Tie2-expressing monocytes, blood "resident" monocytes, and embryonic macrophages suggests common functions and developmental relationships. *Blood* **114**, 901–914 (2009).
22. Smith, L. E. *et al.* Oxygen-induced retinopathy in the mouse. *Invest Ophthalmol Vis Sci* **35**, 101–111 (1994).
23. Banin, E. *et al.* T2-TrpRS inhibits preretinal neovascularization and enhances physiological vascular regrowth in OIR as assessed by a new method of quantification. *Invest Ophthalmol Vis Sci* **47**, 2125–2134 (2006).
24. Smith CA, W. E., O'Maille, G, Abagyan, R, Siuzdak, G. XCMS: processing mass spectrometry data for metabolite profiling using nonlinear peak alignment, matching, and identification. *Anal Chem.*, 779–787 (2006).
25. Nepomuceno, R. R., Pache, L. & Nemerow, G. R. Enhancement of gene transfer to human myeloid cells by adenovirus-fiber complexes. *Mol Ther* **15**, 571–578 (2007).
26. Ritter, M. R. *et al.* Myeloid progenitors differentiate into microglia and promote vascular repair in a model of ischemic retinopathy. *J Clin Invest* **116**, 3266–3276 (2006).
27. Puig-Kroger, A. *et al.* Folate receptor beta is expressed by tumor-associated macrophages and constitutes a marker for M2 anti-inflammatory/regulatory macrophages. *Cancer Res* **69**, 9395–9403 (2009).
28. Gordon, S. & Taylor, P. R. Monocyte and macrophage heterogeneity. *Nat Rev Immunol* **5**, 953–964 (2005).
29. Gustafsson, C. *et al.* Gene expression profiling of human decidual macrophages: evidence for immunosuppressive phenotype. *PLoS One* **3**, e2078 (2008).
30. Docke, W. D. *et al.* Monocyte deactivation in septic patients: restoration by IFN-gamma treatment. *Nat Med* **3**, 678–681 (1997).
31. Gugliesi, F. *et al.* Up-regulation of the interferon-inducible IFI16 gene by oxidative stress triggers p53 transcriptional activity in endothelial cells. *J Leukoc Biol* **77**, 820–829 (2005).
32. El Kasmi, K. C. *et al.* General nature of the STAT3-activated anti-inflammatory response. *J Immunol* **177**, 7880–7888 (2006).

33. Panopoulos, A. D. *et al.* STAT3 governs distinct pathways in emergency granulopoiesis and mature neutrophils. *Blood* **108**, 3682–3690 (2006).
34. Reed, M. J., Koike, T., Sadoun, E., Sage, E. H. & Puolakkainen, P. Inhibition of TIMP1 enhances angiogenesis in vivo and cell migration in vitro. *Microvasc Res* **65**, 9–17 (2003).
35. Siems, W. *et al.* Oxidative stress in chronic renal failure as a cardiovascular risk factor. *Clin Nephrol* **58 Suppl 1**, S12–19 (2002).
36. Smith, L. L. & Johnson, B. H. Biological activities of oxysterols. *Free Radic Biol Med* **7**, 285–332 (1989).
37. Vaya, J. & Schipper, H. M. Oxysterols, cholesterol homeostasis, and Alzheimer disease. *J Neurochem* **102**, 1727–1737 (2007).
38. Bjorkhem, I., Cedazo-Minguez, A., Leoni, V. & Meaney, S. Oxysterols and neurodegenerative diseases. *Mol Aspects Med* **30**, 171–179 (2009).
39. Gordon, S. Alternative activation of macrophages. *Nat Rev Immunol* **3**, 23–35 (2003).
40. Mantovani, A., Sica, A. & Locati, M. New vistas on macrophage differentiation and activation. *Eur J Immunol* **37**, 14–16 (2007).
41. Kodelja, V. *et al.* Differences in angiogenic potential of classically vs alternatively activated macrophages. *Immunobiology* **197**, 478–493 (1997).
42. Pollard, J. W. Trophic macrophages in development and disease. *Nat Rev Immunol* **9**, 259–270 (2009).
43. Fairweather, D. & Cihakova, D. Alternatively activated macrophages in infection and autoimmunity. *J Autoimmun* **33**, 222–230 (2009).
44. Hoefer, I. E. *et al.* Leukocyte subpopulations and arteriogenesis: specific role of monocytes, lymphocytes and granulocytes. *Atherosclerosis* **181**, 285–293 (2005).
45. Otani, A. *et al.* Bone marrow-derived stem cells target retinal astrocytes and can promote or inhibit retinal angiogenesis. *Nat Med* **8**, 1004–1010 (2002).
46. Otani, A. *et al.* Rescue of retinal degeneration by intravitreally injected adult bone marrow-derived lineage-negative hematopoietic stem cells. *J Clin Invest* **114**, 765–774 (2004).
47. Mantovani, A., Sozzani, S., Locati, M., Allavena, P. & Sica, A. Macrophage polarization: tumor-associated macrophages as a paradigm for polarized M2 mononuclear phagocytes. *Trends Immunol* **23**, 549–555 (2002).
48. Mantovani, A. *et al.* The chemokine system in diverse forms of macrophage activation and polarization. *Trends Immunol* **25**, 677–686 (2004).
49. Brichard, B. *et al.* Intracellular cytokine profile of cord and adult blood monocytes. *Bone Marrow Transplant* **27**, 1081–1086 (2001).
50. Gordon, S. & Martinez, F. O. Alternative activation of macrophages: mechanism and functions. *Immunity* **32**, 593–604 (2010).

Acknowledgements

We would like to thank Jeffrey Friedlander for assistance with metabolite treatment, Michele Gerhart for preparing the reference library and Matthew Ritter for helpful discussions. This work was supported by grants to MF from the National Eye Institute (EY11254 and EY017549) and the V. Kann Rassmussen Foundation.

Author contributions

VM and OY conducted the experiments and helped writing the manuscript. EA helped with retina tissue preparation. MW helped with the experiments of immunohistochemistry and confocal imaging. DF helped with cell purification and injection. SM helped with the cytokine profile analysis. KS and MZ performed the Real Time PCR analysis. SN helped with the adenovirus infection. GN reviewed the manuscript and supervised the viral infection studies. GS reviewed the manuscript and supervised the metabolomic studies. MF supervised the study and wrote the manuscript.

Additional information

Additional informations Competing financial interests The authors declare no competing financial interests.

Supplementary information accompanies this paper at http://www.nature.com/scientificreports

How to cite this article: Marchetti, V. *et al.* Differential Macrophage Polarization Promotes Tissue Remodeling and Repair in a Model of Ischemic Retinopathy. *Sci. Rep.* **1**, 76; DOI:10.1038/srep00076 (2011).